Supporting materials

Achieving ultrahigh energy storage performance in bismuth magnesium titanate film capacitors via amorphous-structured engineering

Juan Xie[†], Hanxing Liu[‡], Zhonghua Yao[†,]*, Hua Hao[†], Yanjiang Xie[†], Zongxin Li[†], Minghe Cao[†], Shujun Zhang[§]

[†] State Key Laboratory of Advanced Technology for Materials Synthesis and Processing, School of Material Science and Engineering, Wuhan University of Technology, Wuhan 430070, China.

[‡] State Key Laboratory of Advanced Technology for Materials Synthesis and Processing, International School of Material Science and Engineering, Wuhan University of Technology, Wuhan 430070, China.

[§] Institute for Superconducting and Electronic Materials, Australian Institute of Innovative Materials, University of Wollongong, Wollongong, New South Wales, Australia.

Corresponding Author

* E-mail: yaozhhua@whut.edu.cn

The following is to explain why residual TiO_2 exists in amorphous state instead of crystalline state. In this case, both pure TiO_2 film and BMTx thin films were prepared by sol-gel method at the same annealing temperature (640 °C). Here, we prepared pure TiO_2 film and BMTx (x=0.65) thin film annealed at 560 °C to compare phase structure with that annealed at 640 °C. As shown in the Figure 1S, TiO_2 annealed at 560 °C exists in amorphous form without any diffraction peak while BMTx (x=0.65) shows clear crystalline diffraction peaks. It can be concluded that the BMTx film is preferentially nucleated and crystallized to pure TiO_2 film with increasing annealing temperatures. Crystal growth is a kinetic process which requires the diffusion of growth species of Ti sources. After crystalline phases of the BMTx film form, the residual Ti is separated by crystalline phase of BMTx which inhibits the contact and diffusion of residual Ti to further form crystalline TiO_2 phases.
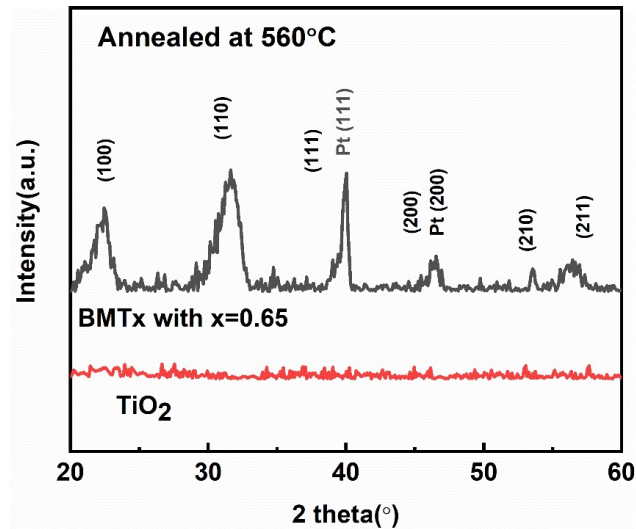

Figure 1S XRD-spectra of BMTx(x=0.65) and pure TiO_2 films annealed at 560 ℃.

As shown in Figure 2S, the HAADF image shows the thickness of BMTx (x=0.65) thin film about 120 nm. In order to confirm the instinct elemental distributions inside and outside the crystalline clusters of BMTx (x=0.65), EDS spectrum is characterized and shown in Figure 2S. It can be observed that elemental distributions inside and outside the crystalline clusters of BMTx (x=0.65) thin film are homogeneous.
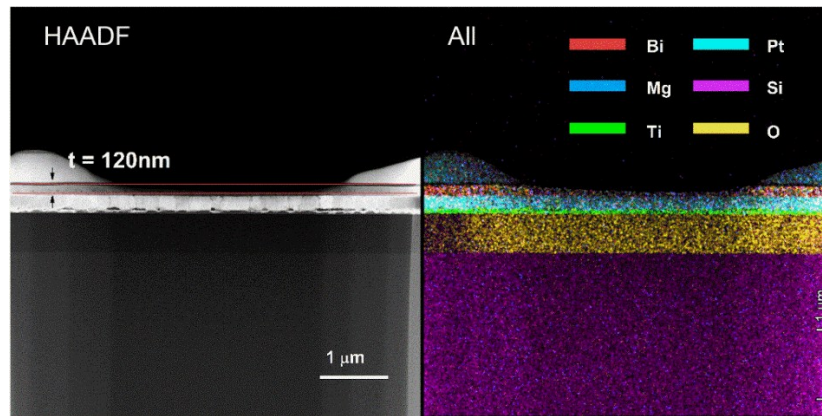
Figure 2S TEM cross section microstructure image and EDS spectrum of the BMTx(x=0.65) films.

Figure 3S shows atomic force microscope image of BMTx films (x=0.70-0.85) under smaller scale compared to Figure 3 in the manuscript. It can be observed that grain size decreases gradually with increasing Ti content. The root mean square roughness of BMTx films is listed in Table 1S. A root mean square roughness of BMTx film is gradually reduced to less than 10 nm at x≥0.65.
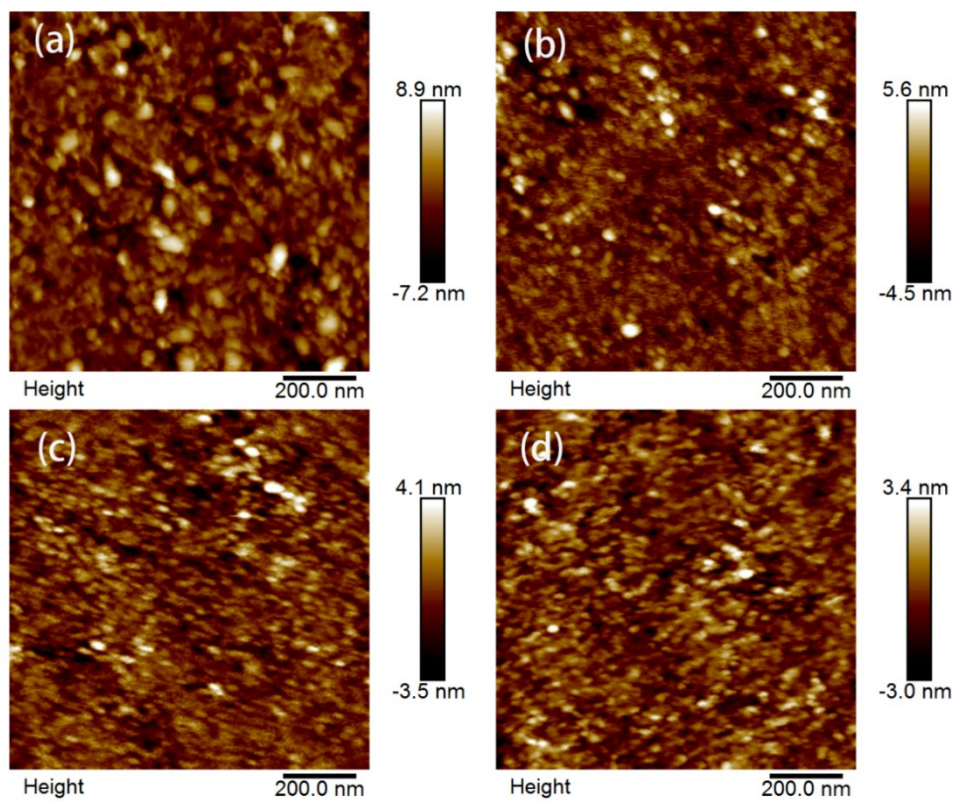

Figure 3S Atomic force microscope image of BMTx films, (a) x=0.70; (b) x=0.75; (c) x=0.80; (d) x=0.85.

Table 1S. Root mean square roughness of $BiMg_{0.5}Ti_xO_3$ films.

Composition x	Rq（nm）	Composition x	Rq（nm）
0.50	33.5	0.70	3.24
0.55	17.3	0.75	2.4
0.60	11.3	0.80	1.93
0.65	9.29	0.85	1.89

Room-temperature *P-E* hysteresis loops of BMTx films were measured under various electric fields at 100 Hz, displayed in Figure 4S. All dielectric films show slim hysteresis loops, indicating that these films possess low energy loss suitable for energy storage application. The E_{max} increases from 900 kV/cm at x=0.50 to 5000 kV/cm at x≥0.80, while maximum polarization P_{max} drastically reduced for x≥0.65.
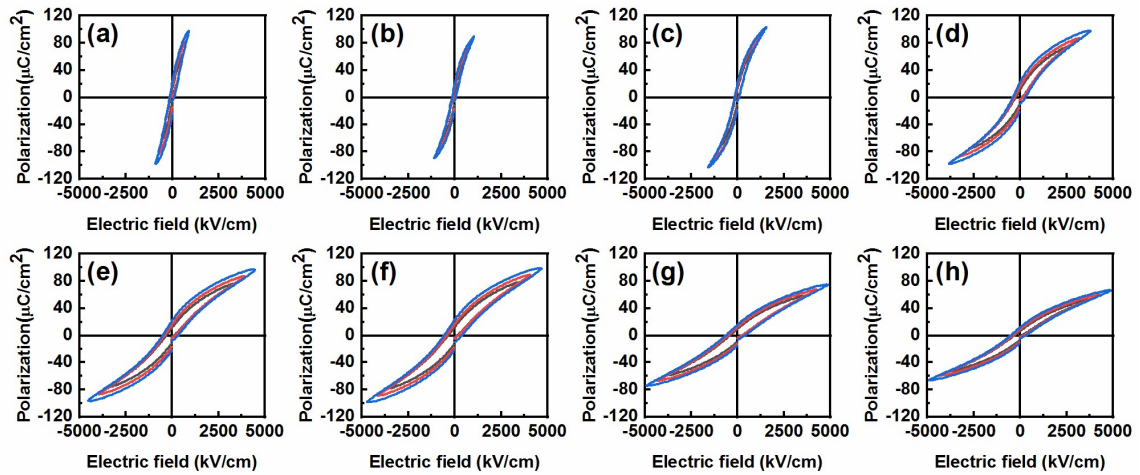

Figure 4S Room-temperature polarization-electric field (*P-E*) hysteresis loops of the BMTx films at 100 Hz, (a) x=0.50; (b) x=0.55; (c) x=0.60; (d) x=0.65; (e) x=0.70; (f) x=0.75; (g) x=0.80; (h) x=0.85.

Figure 5S depicts the leakage characteristics of the BMTx films at room temperature. As shown, the leakage current increases with increasing applied field. Ti-rich films show low leakage current compared with pure perovskite-type $Bi(Mg_{0.5}Ti_{0.5})O_3$ thin film. The inserted Figure 5S (b) shows the linear relationship between log*J* and log*V*. The fitting slope of all samples is close to 1.0, indicating that the conduction mechanism within the film is ohmic contact in the testing voltage
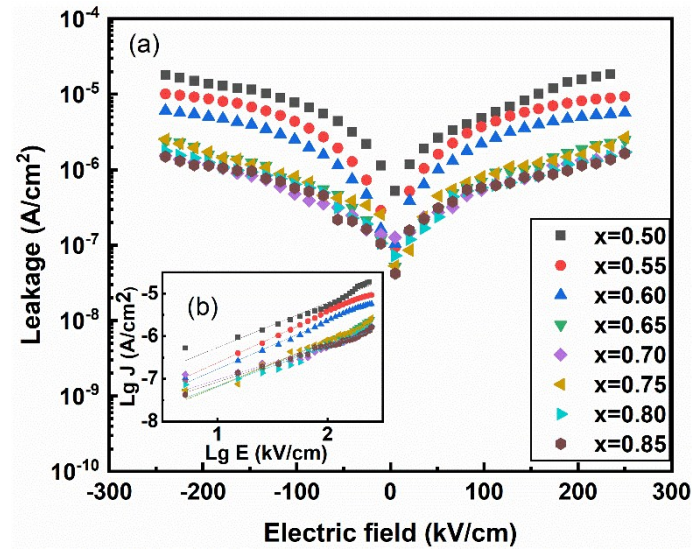
range.

Figure 5S (a) The leakage current of the BMTx films at room temperature under different electric fields; (b) A linear fitting of lg$J$ versus lg$V$ according to the leakage current in Figure 5S(b).

For comparison, P_{max} under the same electric field of 900 kV/cm was plotted in Figure 6S to show the difference of ferroelectric polarization with x. As shown in the figure, P_{max} decreases sharply with increasing x.
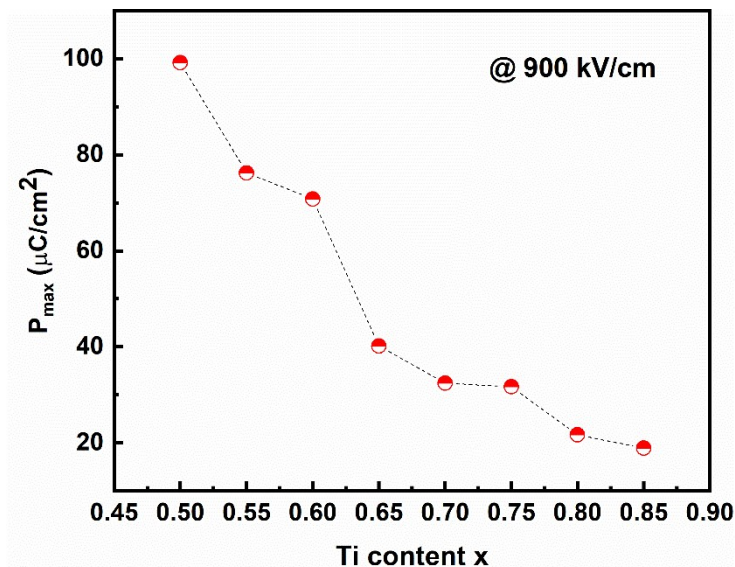

Figure 6S The P_{max} of BMTx films under 900 kV/cm as a function of Ti content x.

Figure 7S shows P-E hysteresis loops of BMTx (x=0.75) thin film under 4000 kV/cm measured

over the temperature of 20-190 °C. As shown in Figure 7, recoverable energy density W_{reco} of BMTx (x=0.75) thin film decreases from 104 J/cm³ at 25 °C to 96 J/cm³ at 190 °C, while ΔW_{reco} value between 0-8% among testing temperatures. This indicates that the BMTx (x=0.75) thin film exhibits excellent thermal stability of energy storage which is suitable for high temperature (till to 190 °C) capacitor applications.
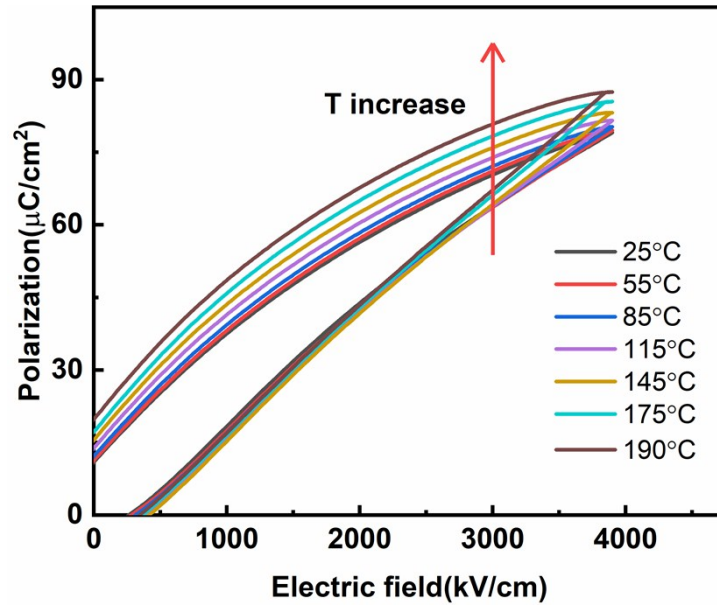

Figure 7S *P-E* hysteresis loops of BMTx (x=0.75) thin film under 4000 kV/cm measured at different temperatures.